3.4 ANALYSIS OF A COLD-AIR PRECIPITATION EVENT: OBSERVATIONAL DIAGNOSIS AND NUMERICAL MODEL SENSITIVITY

Michael J. Brennan* and Gary M. Lackmann
North Carolina State University, Raleigh, North Carolina

1. MOTIVATION AND BACKGROUND

Previous research has shown that latent heating associated with an area of precipitation that developed over the southeastern United States early on 24 January 2000 (Fig. 1) initially generated a lower-tropospheric potential vorticity (PV) maximum that was critical to the downstream moisture transport into the region of heavy snowfall in the 24–25 January 2000 east coast cyclone over the Carolinas and Virginia (Brennan and Lackmann 2005; hereafter BL05). This precipitation feature was termed "incipient precipitation" (IP) by BL05 since it developed prior to the rapid cyclogenesis associated with this event.

The proper representation of latent heating, especially from convective processes, can be critical to the ability of NWP models to predict the genesis and evolution of extratropical cyclones (e.g., Tracton 1973; Bosart 1981; Gyakum 1983a,b; Uccellini et al. 1987; Dickinson et al. 1997). The relationship between latent heating and cyclones is succinctly represented in the framework of PV, as diabatic PV redistribution can result in the enhancement of a downstream upper-tropospheric anticyclone, as well as the generation of a PV maximum in the lower troposphere. This lower-tropospheric PV maximum can represent a critical component in the cyclone dynamics (e.g., Davis and Emanuel 1991; Reed et al. 1992; Stoelinga 1996), as well as significantly alter or enhance lower-tropospheric moisture transport (e.g., Whitaker et al. 1988; Lackmann and Gyakum 1999; Lackmann 2002; BL05).

The diabatic redistribution of PV is governed largely by the horizontal and vertical distribution of latent heating; therefore, if a NWP model does not properly forecast the magnitude and horizontal and vertical distribution of an area of latent heating, there will be associated errors in the PV distribution that could impact both the cyclone evolution and moisture transport. BL05 showed that the proper representation of the IP feature and its associated latent heating was critical to the successful prediction of heavy precipitation over the Carolinas and Virginia in this cyclone event.

The IP was not predicted in 6–12 h forecasts from the 00 UTC 24 January 2000 operational runs of the National Centers for Environmental Prediction's (NCEP) North American Mesoscale (NAM, formerly Eta) and Global Forecast System (GFS, formerly AVN) models even though it occurred over land within and downstream of a region of relatively high data density. Why were the operational models unable to predict the IP feature in the 6–12 h time range?

Numerous surface observations of thunder prior to 12 UTC 24 Jan. over Alabama and Georgia and the cellular nature of radar echoes associated with the IP suggest that convection was occurring within the IP, even though the lower-tropospheric airmass in the region of IP formation was very stable. Elevated convection can occur when surface-based convection moves over a frontal inversion (e.g., Coleman 1990) or when frontogenetical forcing lifts parcels to their lifted condensation level above a stable surface layer (e.g., Martin 1998). Elevated convection can be associated with elevated gravitational instability or symmetric instability, and symmetric instability has been shown to be an important factor in the organization of banded precipitation in numerous cases (e.g., Bennetts and Hoskins 1979; Sanders and Bosart 1985; Thorpe and Emanuel 1985; Wiesmueller and Zubrick 1998; Nicosia and Grumm 1999; Novak et al. 2004).

Conditional symmetric instability (CSI) is present when saturated equivalent-potential temperature (θ_e*) decreases along a surface of constant geostrophic absolute momentum (M_g), or if the saturated geostrophic PV (MPV_g*) is negative (Schultz and Schumacher 1999). The release of CSI is conditional upon saturation, and may occur in situations where gravitational conditional instability (CI) is also present, a circumstance termed convective-symmetric instability by Jascourt et al. (1988). In a case where both CI and CSI are present, it is assumed that gravitational convection will dominate over slantwise convection if it is initiated (Bennetts and Sharp 1982).

To examine the nature of the IP feature, the forcing, moisture, and instability associated with the precipitation formation will be assessed with observations and high-frequency gridded model analyses. Short-range forecasts from the operational Eta model will be evaluated in an effort to determine why the operational models were unable to forecast the IP. Finally, a numerical model simulation will be performed in order to examine the sensitivity of model representation of the IP to model grid spacing.

* *Corresponding author address:* Michael J. Brennan, North Carolina State University, Dept. of Marine, Earth and Atmospheric Sciences, Raleigh, NC 27695;
email: mike_brennan@ncsu.edu

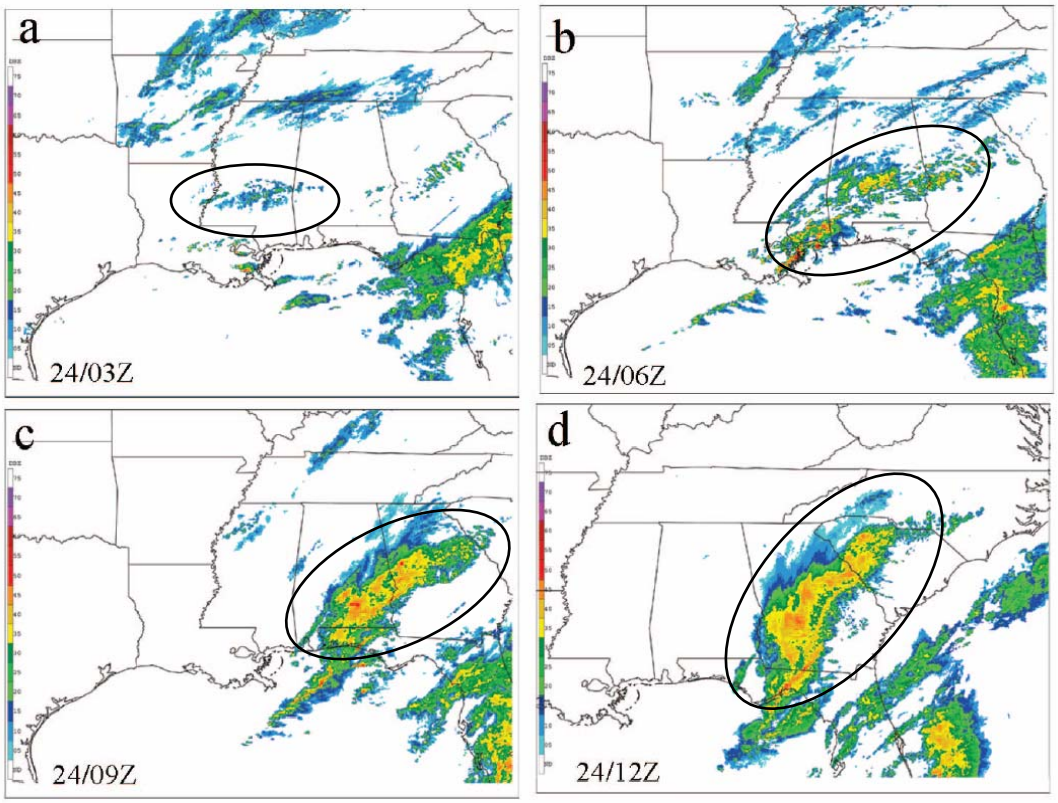

Figure 1. Composite 2-km radar reflectivity imagery at (a) 03 UTC, (b) 06 UTC, (c) 09 UTC, and (d) 12 UTC 24 January 2000. The approximate location of the IP is indicated by the black oval.

2. OBSERVATIONAL ANALYSIS

Available observational data and hourly analyses from the Rapid Update Cycle (RUC) model (Benjamin et al. 1998) were used to document formation and early evolution of the IP feature, which developed over Mississippi beginning around 03 UTC (Fig. 1a), and quickly expanded in coverage and intensity into Alabama and Georgia by 12 UTC 24 January (Fig. 1b,c,d). At 03 UTC, cold surface temperatures indicated that a stable lower-tropospheric airmass existed north of a front that extended along the Gulf Coast (not shown). The 00 UTC 24 January sounding from Jackson, Mississippi, confirms this stable surface layer with a lifted index of +11 (Fig. 2). However, dry air in the mid-troposphere and moist air below indicates the presence of potential instability in the column, which is confirmed by a profile of θ_e constructed from the sounding (not shown).

At 06 UTC, radar imagery and the RUC analysis show that the IP is aligned with an 850-hPa frontogenesis maximum that stretches from southern Mississippi into central Alabama (Fig. 3). At the 500-hPa level, convergence of 500-hPa **Q**-vectors and quasigeostrophic omega values exceeding –9 μb s^{-1} in Mississippi and western Alabama ahead of the upper trough show synoptic-scale forcing for ascent across the region (Fig. 4).

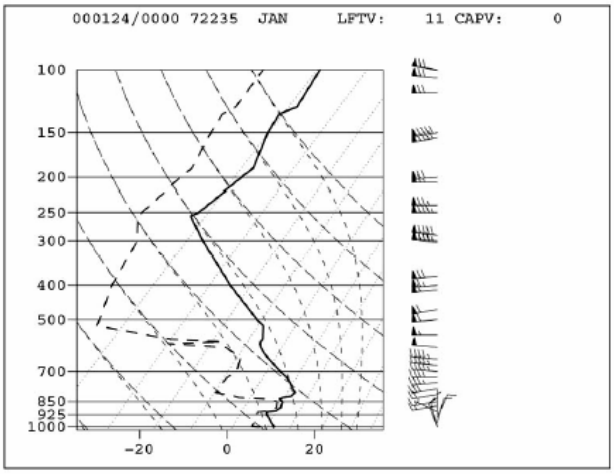

Figure 2. Upper-air sounding valid at 00 UTC 24 Jan. from Jackson, Mississippi. Winds are in kt.

A cross-section taken from the RUC analysis through the large scale baroclinic zone shows a frontogenesis maximum sloping from the surface into the mid-troposphere (Fig. 5a). Instability is prevalent throughout the lower and mid-troposphere above the 850-hPa level with CI present in the southern half of the section where θ_e* decreases with height over a deep layer, while farther north θ_e* is nearly constant with height, with

negative values of MPV_g* indicating the presence of CSI (Fig. 5b). The near-saturated conditions along and above the frontal zone suggest that air parcels would realize this instability as they ascend moist adiabatically in the presence of the synoptic-scale forcing for ascent over the region. The combination of widespread synoptic-scale ascent and the potentially unstable thermodynamic configuration noted above are consistent with the development of convection in the region of interest.

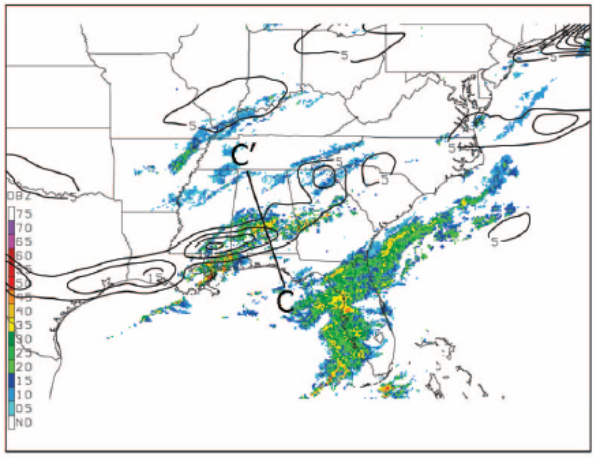

Figure 3. RUC model analysis at 06 UTC 24 Jan. of (a) 850-hPa frontogenesis (solid contours every 5 × 10^{-1} °C 100 km^{-1} 3 h^{-1}) with radar mosaic imagery. Solid line C–C' indicates cross-section displayed in Fig. 5.

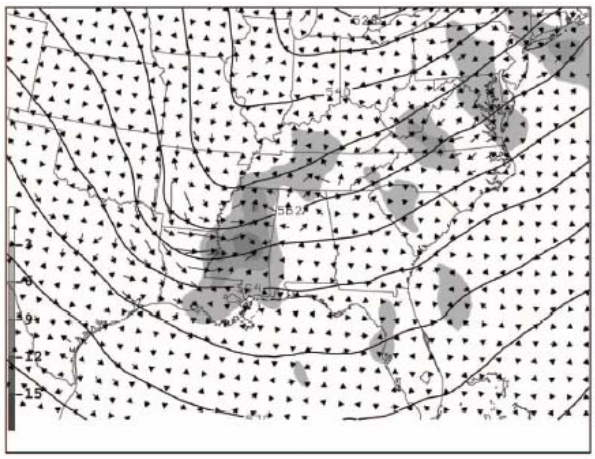

Figure 4. RUC model analysis at 06 UTC 24 Jan. of 500-hPa Q-vectors (arrows), 500-hPa quasigeostrophic vertical velocity (shading every 3 μb s^{-1} shows upward motion), and 500-hPa geopotential height (solid contours every 6 dam).

3. OPERATIONAL MODEL EVALUATION

The same cross section from the 6-h forecast of the NCEP Eta model (Fig. 5c,d) is compared to the 06 UTC 24 Jan. RUC analysis (Fig. 5a,b). The Eta forecast shows weaker ascent over a region of weaker frontogenesis (Fig. 5c), with the magnitude and extent of the CSI in the Eta forecast in the 850–750-hPa layer reduced. The weaker warm tongue in the θ_e* field results in less negative values of MPV_g* and a general decrease in the magnitude of instability (Fig. 5d). The combination of weaker vertical motion and a lack of saturated conditions above the frontal inversion make it less likely for the weaker instability to be realized and is consistent with the lack of precipitation formation in the Eta forecast.

Persson and Warner (1993) found that horizontal grid spacing of 6–15 km and vertical grid spacing of 70–170 m were required for a model to fully resolve the most unstable growth mode associated with CSI. Therefore, the ability of the Eta model at the time of this event to properly capture the effects of elevated slantwise convection is doubtful, as the configuration of the Eta model at this time (32-km horizontal grid spacing) falls well short of the aforementioned threshold, and the Eta does not parameterize slantwise convection. Also, at the time of this event the Betts-Miller-Janjić CP scheme used in the Eta model only examined the lowest 130 hPa of the atmosphere for instability (Manikin et al. 2000), and would not trigger if gravitational instability was located above this level. Given this evidence, it is unlikely that the Eta model would be able to fully capture the effects of any elevated convection (gravitational or slantwise) associated with the IP, precluding it from generating the latent heat release associated with the IP and its impacts on the PV distribution that were shown by BL05 to be critical to the evolution of this case.

4. SENSITIVITY TO MODEL GRID SPACING

The sensitivity of the ability of an NWP model to simulate the IP formation with respect to grid spacing was tested with a nested simulation using version 2.0.3.1 of the Weather Research and Forecast (WRF) model with the Advanced Research WRF (ARW) dynamical core developed at NCAR (Skamarock et al. 2005). The outer (inner) domain was run with 12-km (4-km) horizontal grid spacing (Fig. 6), and the Kain-Fritsch (no) CP scheme. Both domains had 59 vertical levels. The simulation was initialized at 00 UTC from the RUC analysis, with no feedback was provided to the outer grid from the inner domain.

To examine the sensitivity of the initial formation of the IP to horizontal grid spacing, the output from the 4-km simulation is compared to that from the 12-km simulation. Simulated radar reflectivity at the 700-hPa level from the 4-km simulation shows the development of precipitation echoes over central Alabama by 07 UTC (Fig. 7). A cross section taken along line D–D' through these echoes from the 4-km simulation shows three maxima of simulated reflectivity, two exceeding 20 dBZ near the 650-hPa level (Fig. 8a).

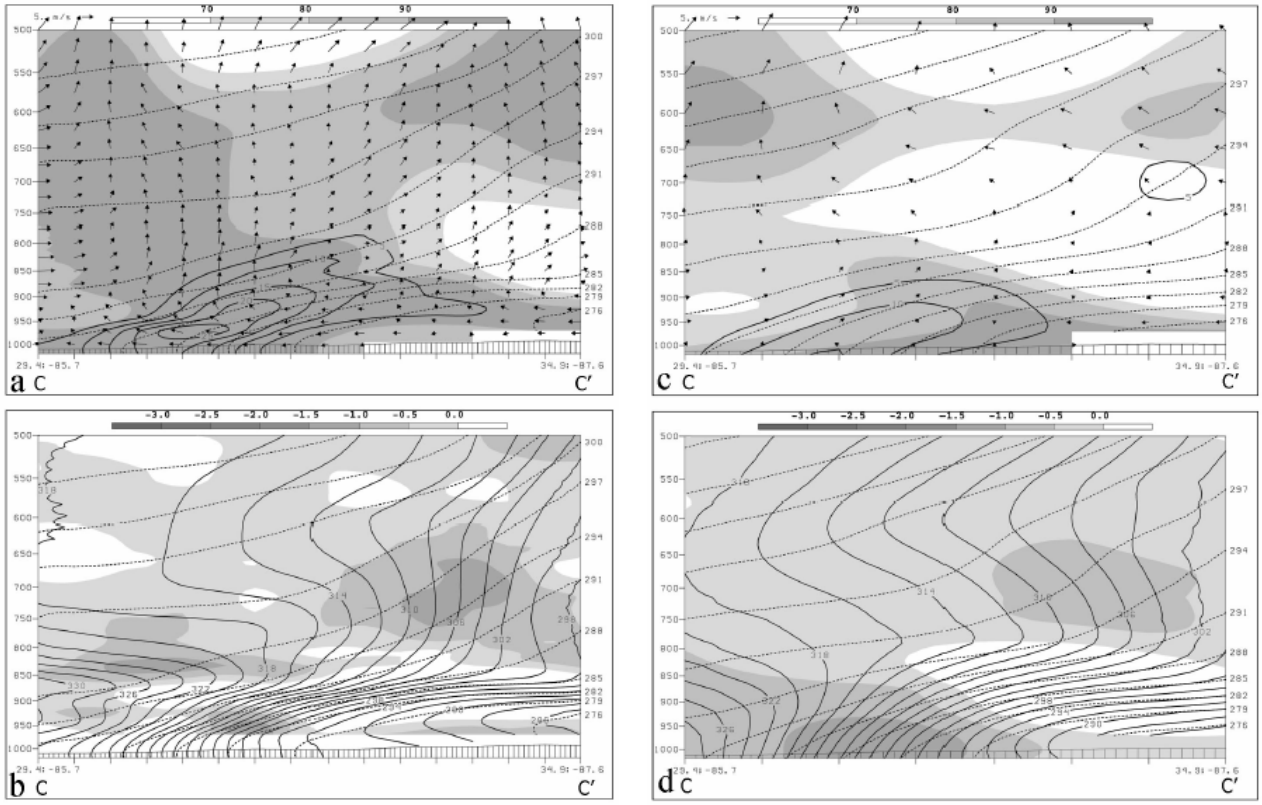

Figure 5. Cross-section from 29.4°N 85.7°W to 34.92°N 87.6°W (along line C–C' in Fig. 3) at 06 UTC 24 Jan. showing (a) RUC model analysis of relative humidity (shaded above 70%), frontogenesis (solid contours every 5 × 10^{-1} °C 100 km^{-1} 3 h^{-1}), potential temperature (dashed contours every 3 K) and ageostrophic circulation (arrows); (b) saturated geostrophic potential vorticity (MPV_g^*, negative values shaded every 0.5 PVU; where 1 PVU = 1.0 ×10^{-6} m^2 s^{-1} K kg^{-1}), potential temperature (dashed contours every 3 K), and saturated equivalent-potential temperature (θ_e*, solid contours every 2 K); (c) and (d), as in (a) and (b), except 6-h Eta model forecast valid at 06 UTC 24 Jan.

A band of instability where values of MPV_g* are less than –2 PVU is noted between 650 and 600 hPa across the left half of the section, with a region where MPV_g* values are less than –5 PVU to the left of the largest echo. The upward vertical velocity increases markedly above this unstable layer where θ_e* is decreasing along M_g surfaces above the tongue of low θ_e^* values centered near the 650-hPa level (Fig. 8b). The location of the precipitation echoes and vertical velocity maxima corresponds closely to the regions where elevated CSI is indicated in the cross section, consistent with that seen in the RUC analysis at 06 UTC (Fig. 5a,b).

The same cross section from the 12-km simulation at this time shows that the intensity of the echoes and vertical velocity is reduced, especially near the center of the section (Fig. 8c,d). In the 650–600-hPa layer, the M_g surfaces (Fig. 8d) are more parallel to the θ_e* surfaces relative to the 4-km simulation (Fig. 8b), resulting in reduced instability in this layer on the left side of the section (Fig. 8c). Also, in the 600–450-hPa layer, θ_e* is increasing with height in the center of the section in the 12-km simulation (Fig. 8d), while weak gravitational conditional stability is seen in this layer in

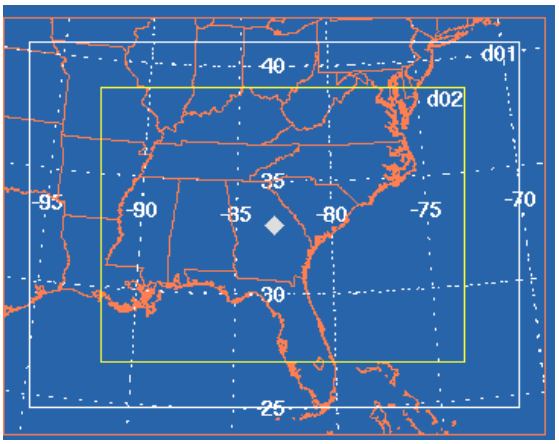

Figure 6. Horizontal extent of 12-km (d01) and 4-km (d02) domains used in WRF simulation.

the 4-km simulation (Fig. 8b) where θ_e* is nearly constant with height. These findings are consistent with the reduced upward vertical velocity and reflectivity in the 12-km simulation at this time. The evolution of the

precipitation, vertical velocity, and stability fields in these simulations strongly suggest that elevated CSI and gravitational CI played a role in the generation of precipitation echoes aloft across the region of IP formation early on 24 January. The spatial and temporal correlation between the reflectivity and vertical velocity maxima with areas of elevated CSI and CI strongly suggests that parcels were achieving positive buoyancy, initially along slantwise trajectories in the band of CSI above a tongue of low θ_e^*-air.

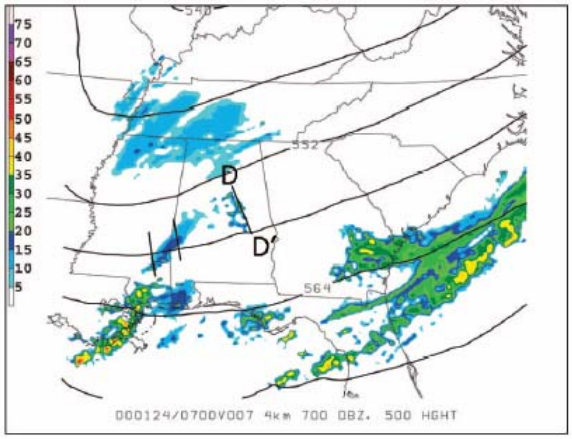

Figure 7. 700-hPa simulated reflectivity (color shading, dBZ) and 500-hPa height (solid contours, dam) from 4-km WRF simulation valid at 07 UTC 24 January 2000. Line D–D' indicates cross sections shown in Fig. 8.

The degraded precipitation structure and weaker vertical velocity seen in the 12-km simulation relative to the 4-km simulation is consistent with Persson and Warner (1993) who found that models with larger grid spacing were able to resolve CSI induced circulations, but their onset would be delayed and their intensity degraded. The amount of degradation seen here by increasing the grid spacing from 4-km to 12-km suggests that a further increase in grid spacing to the 32 km used in the operational Eta model at the time of this event would reduce the intensity of these CSI circulations and delay their onset time even further, and is consistent with the weaker vertical velocity and lack of precipitation in the Eta forecast.

5. CONCLUSIONS

Observations and data from the RUC analysis show that the cold-air IP feature formed along a zone of lower-tropospheric frontogenesis north of the Gulf Coast as an approaching upper-trough led to increased divergence aloft over the region. Above the frontal inversion, the lower- and mid-troposphere was characterized by negative values of MPV_g^* indicating a deep layer of convective-symmetric instability. The presence of elevated instability combined with sufficient moisture and synoptic-scale forcing for ascent is consistent with the formation and expansion of the precipitation shield with embedded convection over the southeastern United States during the period.

The forecast from the operational Eta model was deficient in both the strength of forcing for ascent and instability in the region. This combination likely contributed to the model's inability to generate this area of precipitation, its associated lower-tropospheric PV maximum and the subsequent precipitation distribution in the Carolinas and Virginia.

A WRF model simulation performed to examine the sensitivity of model IP forecasts with regard to grid-spacing found that the magnitude of the instability, vertical velocity and simulated reflectivity was decreased as grid spacing increased. This suggests that a model's ability to represent the elevated instability and its impact on the formation of the IP in this event is strongly sensitive to horizontal and vertical grid spacing, and is consistent with the inability of the even coarser operational Eta model to generate the IP feature.

Since current operational NWP models are still run with CP schemes and have insufficient grid spacing to properly resolve the effects of slantwise convection, the potential exists for cases to occur where operational models may be unable to represent a cold air precipitation feature associated with elevated gravitational and slantwise instability. This could result in an erroneous representation of the lower-tropospheric PV distribution, possibly degrading forecasts of downstream moisture transport and cyclone evolution. Operational forecasters should be aware of this and use available observations and high-frequency model analyses to evaluate model forecasts of precipitation and the impact of latent heating on the PV distribution. This, in combination with an understanding of the potential feedbacks from precipitation (in NWP models and in reality) onto atmospheric dynamics could allow forecasters to know when and how to adjust model guidance to hopefully improve forecasts of potentially high-impact events.

6. ACKNOWLEDGEMENTS

This research was supported by NOAA Collaborative Science, Technology, and Applied Research (CSTAR) Grants NA03NWS4680007 and NA-07WA0206, and NSF Grant ATM-0342691, all awarded to North Carolina State University. NCEP provided much of the meteorological data used in this study, which was delivered to North Carolina State University through the Unidata program. Additional RUC-model data were obtained from the Atmospheric Radiation Measurement (ARM) Program sponsored by the U.S. Department of Energy, Office of Science, Office of Biological and Environmental Research, Environmental Sciences Division. The WRF model was made available through NCAR, which is sponsored by the NSF. Mr. Ryan Torn of the University of Washington provided the original code to convert WRF output to GEMPAK.

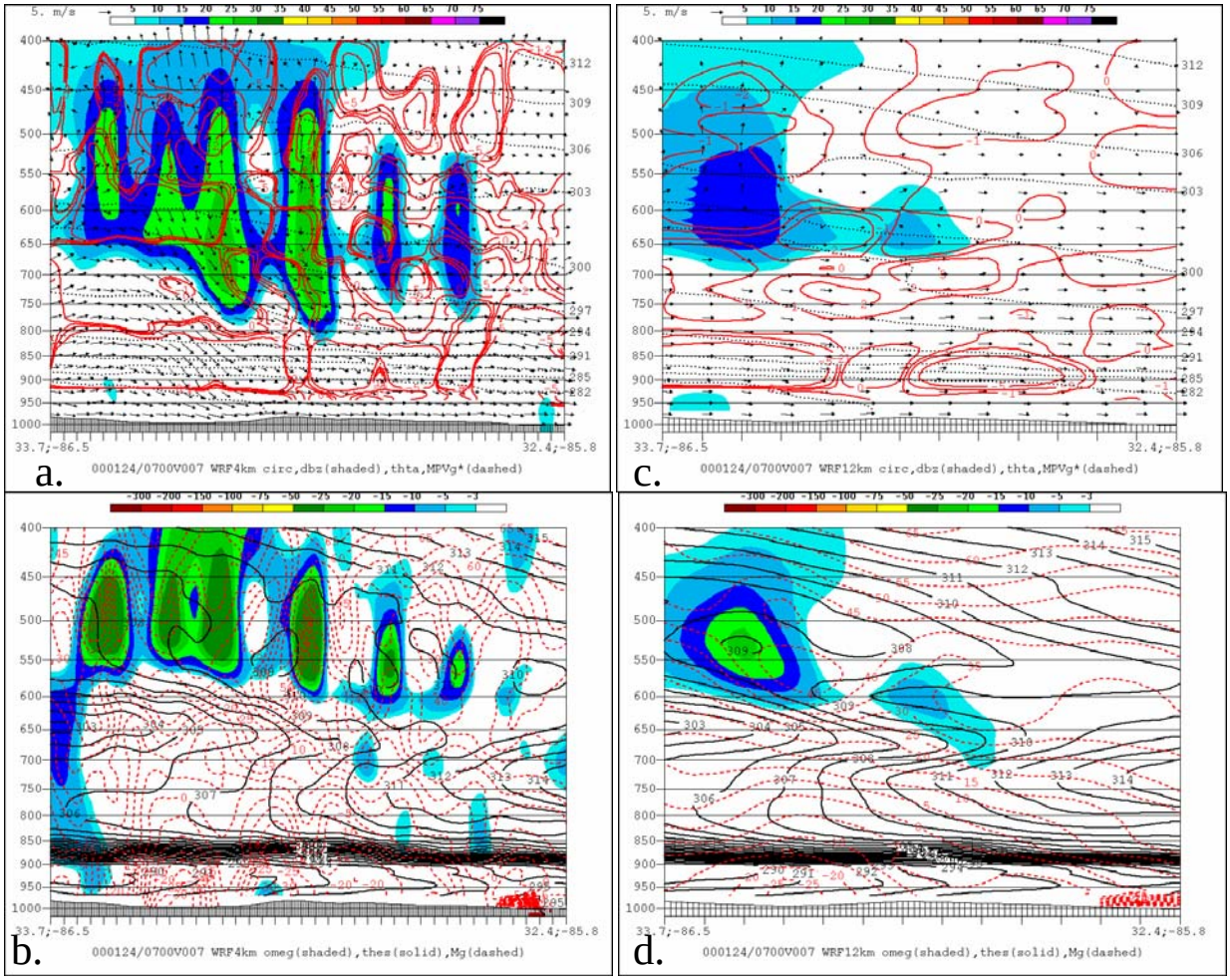

Figure 8. Cross section along a line from 33.7ºN 86.5ºW to 32.4ºN 85.8ºW (depicted by line D–D' in Fig. 7) from 4-km WRF simulation at 07 UTC 24 January showing (a) simulated radar reflectivity (color shading, dBZ), total circulation (arrows m s^{-1}), potential temperature (dotted black contours every 3 K) and saturated geostrophic potential vorticity (0, –1, –2, and –5 PVU values depicted by solid red contours); (b) upward vertical velocity (color shading, μb s^{-1}), saturation equivalent potential temperature (solid black contours every 1 K), and absolute geostrophic momentum surfaces (dotted red contours every 5 m s^{-1}); (c) and (d) as in (a) and (b), except from 12-km WRF simulation.

7. REFERENCES

Benjamin, S. G., J. M. Brown, K. J. Brundage, B. E. Schwartz, T. G. Smirnova, T. L. Smith, L. L. Morone, 1998: RUC-2 - The Rapid Update Cycle Version 2. NWS Technical Procedures Bulletin No. 448. National Oceanic and Atmospheric Administration, U.S. Department of Commerce, 18 pp. [Available online at http://www.nws.noaa.gov/om/tpb/448.htm].

Bennetts, D. A., and B. J. Hoskins, 1979: Conditional symmetric instability–A possible explanation for frontal rainbands. *Quart. J. Roy. Meteor. Soc.,* **105,** 945–962.

———, and J. C. Sharp, 1982: The relevance of conditional symmetric instability to the prediction of mesoscale frontal bands. *Quart. J. Roy. Meteor. Soc.,* **108,** 595–602.

Bosart, L. F., 1981: The Presidents' Day snowstorm of 18–19 February 1979: A sub-synoptic scale event. *Mon. Wea. Rev.,* **109,** 1542–1566.

Brennan, M. J., and G. M. Lackmann, 2005: The influence of incipient latent heat release on the precipitation distribution of the 24–25 January 2000 cyclone. *Mon. Wea. Rev.,* **133,** 1913–1937.

Colman, B. R., 1990: Thunderstorms above frontal surfaces in environments without positive CAPE. Part II: Organization and instability mechanisms. *Mon. Wea. Rev.,* **118,** 1123–1144.

Davis, C. A., and K. A. Emanuel, 1991: Potential vorticity diagnostics of cyclogenesis. *Mon. Wea. Rev.,* **119,** 1929–1953.

Dickinson, M. J., L. F. Bosart, W. E. Bracken, G. J. Hakim, D. M. Schultz, M. A. Bedrick, and K. R. Tyle, 1997: The March 1993 Superstorm: Incipient phase synoptic- and convective-scale flow interaction and model performance. *Mon. Wea. Rev.,* **125,** 3041–3072.

Gyakum, J. G., 1983a: On the evolution of the *QE II* storm. I: Synoptic aspects. *Mon. Wea. Rev.,* **111,** 1137–1155.

———, 1983b: On the evolution of the *QE II* storm. II: Dynamic and thermodynamic structure. *Mon. Wea. Rev.,* **111,** 1156–1173.

Jascourt, S. D., S. S. Lindstrom, C. J. Seman, and D. D. Houghton, 1988: An observation of banded convective development in the presence of weak symmetric stability. *Mon. Wea. Rev.,* **116,** 175–191.

Lackmann, G. M., 2002: Cold-frontal potential vorticity maxima, the low-level jet, and moisture transport in extratropical cyclones. *Mon. Wea. Rev.,* **130,** 59–74.

———, and J. G. Gyakum, 1999: Heavy cold-season precipitation in the northwestern United States: Synoptic climatology and an analysis of the flood of 17–18 January 1986. *Wea. Forecasting,* **14,** 687–700.

Manikin, G., M. Baldwin, W. Colins, J. Gerrity, D. Keyser, Y. Lin, K Mitchell, and E. Rogers, 2000: Changes to the NCEP meso Eta runs: Extended range, added input, added output, convective changes. NWS Technical Procedures Bulletin 465, National Oceanic and Atmospheric Administration, U.S. Department of Commerce, 84 pp. [Available online at http://www.nws.noaa.gov/om/tpb/465.htm].

Martin. J. E., 1998: The structure and evolution of a continental winter cyclone. Part II: Frontal forcing of an extreme snow event. *Mon. Wea. Rev.,* **126,** 329-348.

Nicosia, D. J., and R. H. Grumm, 1999: Mesoscale band formation in three major northeastern United States snowstorms. *Wea. Forecasting,* **14,** 346–368.

Novak, D. R., L. F. Bosart, D. Keyser, and J. S. Waldstreicher, 2004: An observational study of cold season–banded precipitation in northeast U.S. cyclones. *Wea. Forecasting,* **19,** 993–1010.

Persson. P. O. G., and T. T. Warner, 1993: Nonlinear hydrostatic conditional symmetric instability: Implications for numerical weather prediction. *Mon. Wea. Rev.,* **121,** 1821–1833.

Reed, R. J. M. T. Stoelinga, and Y.-H. Kuo, 1992: A model-based study of the origin and evolution of the anomalously high potential vorticity in the inner region of a rapidly deepening marine cyclone. *Mon. Wea. Rev.,* **120,** 893–913.

Sanders, F., and L. F. Bosart, 1985: Mesoscale structure in the Megalopolitan snowstorm of 11–12 February 1983. Part I: Frontogenetical forcing and symmetric instability. *J. Atmos. Sci.,* **42,** 1050–1061.

Skamarock, W. C., J. B. Klemp, J. Dudhia, D. O. Gill, D. M. Barker. W. Wang, and J. G. Powers, 2005: A description of the Advanced Research WRF Version 2. NCAR Tech. Note, NCAR/TN-468+STR, 100 pp.

Schultz, D. M., and P. N. Schumacher, 1999: The use and misuse of conditional symmetric instability. *Mon. Wea. Rev.,* **127,** 2709–2732; Corrigendum, **128,** 1573.

Stoelinga, M. T., 1996: A potential-vorticity based study of the role of diabatic heating and friction in a numerically simulated baroclinic cyclone. *Mon. Wea. Rev.,* **124,** 849–874.

Thorpe, A. J., and K. A. Emanuel, 1985: Frontogenesis in the presence of small stability to slantwise convection. *J. Atmos. Sci.,* **42,** 1809–1824.

Tracton, M. S., 1973: The role of cumulus convection in the development of extratropical cyclones. *Mon. Wea. Rev.,* **101,** 573–592.

Uccellini, L. W., R. A. Petersen, K. F. Brill, P. J. Kocin, and J. J. Tuccillo, 1987: Synergistic interactions between an upper-level jet streak and diabatic processes that influence the development of a low-level jet and a secondary coastal cyclone. *Mon. Wea. Rev.,* **115,** 2227–2261.

Wiesmueller, J. L, and S. M. Zubrick, 1998: Evaluation and application of conditional symmetric instability, equivalent potential vorticity, and frontogenetic forcing in an operational forecast environment. *Wea. Forecasting,* **13,** 84–101.

Whitaker, J. S., L. W. Uccellini, and K. F. Brill, 1988: A model-based diagnostic study of the rapid development phase of the Presidents' Day cyclone. *Mon. Wea. Rev.,* **116,** 2337–2365.